

1 **Atmospheric Fe supply **might have had** a negligible role in promoting marine**
2 **productivity in the Glacial North Pacific Ocean**

3 Burgay F.^{1,2}, Spolaor A.^{1*}, Gabrieli J.¹, Cozzi G.¹, Turetta C.¹, Vallelonga P.^{3,4}, Barbante C.^{1,2}

4

5 ¹Institute of Polar Sciences, National Research Council. Via Torino, 155, 3100 Venice (Italy)

6 ²Department of Environmental Sciences, Informatics and Statistics, Ca' Foscari University of Venice. Via
7 Torino, 155 – Venice (Italy)

8 ³Physics of Ice Climate and Earth, Niels Bohr Institute, University of Copenhagen. Tagensvej 16,
9 Copenhagen N2200 (Denmark)

10 ⁴Oceans Graduate School, University of Western Australia (Australia)

11 * Corresponding author: andrea.spolaor@unive.it

12 **Abstract**

13 Iron is a key element in the Earth climate system as it can enhance the marine primary productivity in the
14 High-Nutrient Low-Chlorophyll (HNLC) regions where, despite a high concentration of major nutrients, the
15 chlorophyll production is low due to iron limitation. **Aeolian mineral dust represents one of the main Fe**
16 **sources to the oceans; thus, quantifying its variability over the last millennia is crucial to evaluate its role in**
17 **strengthening the biological carbon pump. Polar ice cores, which preserve detailed climate records in their**
18 **stratigraphy, provide a sensitive and continuous archive for reconstructing past Fe fluxes.** Here, we show the
19 Northern Hemisphere Fe record retrieved from the NEEM ice core (**Greenland**), which offers a unique
20 opportunity to reconstruct the past Fe fluxes **in a portion of the Arctic** over the last 108 kyr. Holocene (**0.042**
21 **-11.7 kyr b2k**) Fe fluxes to the Arctic were **four** times lower than the average recorded over the Last Glacial
22 Period (**11.7– 108 kyr b2k**), **while** they were greater during the Last Glacial Maximum (LGM, **14.5 – 26.5**
23 **kyr b2k**) and Marine Isotope Stage 4 (MIS 4, **60 - 71 kyr b2k**). Comparing **the NEEM Fe record** with
24 palaeoceanographic records retrieved from the HNLC North Pacific, **we found that the coldest periods,**
25 **characterized by the highest Fe fluxes, were characterized by a low marine primary productivity** in the

26 subarctic Pacific Ocean, likely due to the greater sea-ice extent and the absence of major nutrients upwelling.
27 This supports the hypothesis that Fe-fertilization during colder and dustier periods (i.e. LGM and MIS 4) was
28 more effective in other regions, such as the mid-latitude North Pacific, where a closer relationship between
29 marine productivity and the NEEM Fe fluxes was observed.

30 1. Introduction

31 Greenland and Antarctic ice cores are unique archives that can provide records of temperature,
32 atmospheric dust load and atmospheric gas composition variability during the Holocene and the late
33 Pleistocene (Jouzel et al., 1996; Lambert et al., 2008; Schüpbach et al., 2018; Watanabe et al., 2003). Glacial
34 periods were dustier and characterized by a lower CO₂ concentration (≈ 180 ppm) than interglacials (≈ 280
35 ppm). This dichotomy is explained through several different hypotheses: the increase in aridity and newly
36 exposed continental shelves (Fuhrer et al., 1999), an increase in the aerosol atmospheric life-time resulted
37 from a reduced hydrological cycle (Lambert et al., 2008; Yung et al., 1996), increased glacial-derived
38 mobilization of highly bioavailable iron (Fe) from physical breakdown of bedrock (Shoenfelt et al., 2018),
39 and, lastly, more vigorous polar circulation capable of entraining additional dust from lower latitudes
40 (Mayewski et al., 1994). Regardless of the source, the higher atmospheric burden of mineral dust during
41 glacial periods affected climate through both physical and biological mechanisms. Dust particles can directly
42 influence the Earth radiative budget by scattering, absorbing and re-emitting shortwave and longwave
43 radiation (Miller and Tegen, 1998; Schepanski, 2018). During the LGM, model results showed that the
44 enhanced dust transport caused, alone, a 1.0 W/m² globally averaged radiative forcing decrease compared to
45 present day conditions, which contributed to a 0.85°C cooling relative to the current climate (Mahowald et
46 al., 2006). Conversely, once deposited on the ocean surface, the mineral dust delivered major and
47 micronutrients (including Fe) that could have stimulated the biological carbon pump (Martin et al., 1990).
48 Indeed, Fe can limit Marine Primary Production (MPP) in the High-Nutrient Low-Chlorophyll (HNLC)
49 oceans, which are characterized by a high concentration of nutrients, but low productivity (Martin et al.,
50 1990). The largest ones are the Southern Ocean, the Equatorial Pacific and the North Pacific Ocean (Duggen
51 et al., 2010). In these regions, the Fe role in modulating marine productivity was demonstrated through both
52 artificial Fe fertilization experiments (Smetacek et al., 2012; Tsuda et al., 2003; Yoon et al., 2018) and
53 natural Fe inputs from iceberg melting, volcanic eruptions and glacially sourced dust (Duprat et al., 2016;

54 Langmann et al., 2010; Shoenfelt et al., 2017). For its biological relevance, it has been hypothesized that the
55 recorded decrease in the atmospheric CO₂ concentration during glacial periods was linked to the Fe-
56 modulated enhancement of the biological carbon pump in the HNLC regions due to the increase in Fe
57 availability (Martin et al., 1990). Evidences for the existence of a strong link between atmospheric Fe
58 deposition and marine productivity were retrieved from a marine sediment core collected in the subantarctic
59 zone of the Southern Ocean where, the coldest periods were mirrored by an increase in atmospheric Fe
60 fluxes and by an enhancement of both MPP and degree of nutrient consumption (Martínez-García et al.,
61 2014). Yet, according to both modeling (Lambert et al., 2015) and observational (Gaspari et al., 2006;
62 Röthlisberger, 2004; Vallelonga et al., 2013) studies, the Fe-fertilization mechanism itself cannot completely
63 explain the ≈100 ppmv glacial-interglacial atmospheric CO₂ variability, but only around 8-20 ppmv of it
64 (Lambert et al., 2015).

65 However, the role of Fe fertilization in the Northern Hemisphere and in the HNLC region of the North
66 Pacific is unclear due to the few available Arctic Fe flux records which are either limited to the last century
67 or they only cover short time periods (Burgay et al., 2019; Hiscock et al., 2013). Thus, reconstructing how
68 the Fe concentrations and fluxes have changed in the Northern Hemisphere in the last millennia is essential
69 to understand the evolution of the global atmospheric circulation, the human impact on dust mobilization
70 (Mahowald et al., 2008) and to evaluate, as well, the impact that Fe might have had on MPP in the North
71 Pacific HNLC region. Here, we present a 108 kyr record of Total Dissolvable Fe (TDFe) retrieved from the
72 North Greenland Eemian Ice Drilling (NEEM) ice core (Rasmussen et al., 2013; Schüpbach et al., 2018),
73 which provides a unique insight on the atmospheric Fe supply in the Arctic both during the Holocene and the
74 Last Glacial Period. Furthermore, we performed a comparison between the TDFe NEEM record and various
75 palaeoproductivity records from the HNLC North Pacific region (Figure 1) to evaluate whether the increase
76 in aeolian Fe fluxes was mirrored by an increase in marine productivity. We underline that, TDFe
77 concentrations, as it will be discussed in the following, derives from the acidification of the snow samples for
78 1 month at pH 1. Thus, they represent an upper limit of the aeolian Fe potentially available for the
79 phytoplankton, and it might overestimate the actual bioavailable Fe.

80 2. Materials and methods

81 **2.1 Sampling and cleaning procedure**

82 In the framework of the NEEM project, a 2540 m-depth ice core was drilled in north-western
83 Greenland (77°45'N, 51°06'W) at 2479 m.a.s.l. The site is characterized by an average annual temperature
84 of -29°C and a modern accumulation of 22 cm ice equivalent per year. According to the GICC05modelext-
85 NEEM-1 timescale, the ice core covers the last 128 kyrs (Rasmussen et al., 2013). The ice cores were cut to
86 obtain ice sticks with a square cross section of 36x36 mm. They were continuously melted on a continuous
87 flow analysis (CFA) system with a typical melt-speed of 3.5 cm min⁻¹ (Schüpbach et al., 2018). The CFA
88 system provides meltwater from the inner and **least likely to be contaminated** part of the core, thus we did
89 not adopt any further decontamination procedure. **The ICP-MS samples were manually collected at a low-**
90 **resolution (110 cm).** The temporal resolution depends on the accumulation rate and it decreases with depth
91 because of the ice thinning. According to the available timescale (Rasmussen et al., 2013) and considering
92 the 110 cm sampling resolution, the temporal resolution varies from decadal to millennial (Table 1).

93 Samples were collected in vials previously cleaned as follows: 7 days with HNO₃ 5% (Suprapure,
94 Romil, UK), rinsed three times with Ultrapure water (UPW, Elga, UK), 7 days with HNO₃ 2% (Suprapure,
95 Romil, UK), rinsed three times with UPW and **then stored in HNO₃ 1% (Ultrapure, Romil, UK) until the day**
96 **before the sample collection, when they were rinsed three times with UPW and dried overnight under a**
97 **laminar flow hood Class 100.** The samples were kept frozen and shipped to Italy for analysis. Once melted,
98 the samples were acidified to pH 1 using HNO₃ (Suprapure, Romil, UK). To ensure an effective dissolution
99 of Fe particles, samples were stored at room temperature and analysed 30 days after the acidification **without**
100 **any additional filtration step. We adopted this approach since the analysis immediately after the acidification**
101 **step might have led to uncertainties attributable to the Fe dissolution kinetics (Edwards, 1999; Koffman et**
102 **al., 2014). Our choice was consistent with other studies that indicate that samples to be used for calculation**
103 **of atmospheric fluxes must be acidified for at least 1 month prior to analysis to avoid any possible**
104 **misinterpretation of the trace-element data (Koffman et al., 2014). We will refer to this fraction as Total**
105 **Dissolvable Fe (TDFe) which includes both the most labile fraction (Dissolved iron, DFe), which is rendered**
106 **soluble under mildly acidic conditions (Hiscock et al., 2013), and the fraction enclosed in iron-bearing**
107 **mineral particles. TDFe does not directly represent the actual bioavailable Fe that can be dissolved into**

108 seawater at pH 8, but, considering that TDFe and DFe are significantly correlated (Du et al., 2020; Xiao et
109 al., 2020), an upper limit of the aeolian Fe potentially available for the phytoplankton (Edwards et al., 2006).

110 2.2 Analytical procedure and performances

111 The ice samples were analysed with an Inductively Coupled Plasma Single Quadrupole Mass
112 Spectrometer (ICP-qMS, Agilent 7500 series, USA) equipped with a quartz Scott spray chamber for the
113 determination of Ca, Na and Fe. To minimize any kind of contamination, all the instrument tubes were
114 flushed before the analysis for 2 hours with 2% HNO₃ (Suprapure, Romil, UK). A 120 seconds rinsing step
115 with 2% HNO₃ (Suprapure, Romil, UK) occurred after each sample analysis to reduce any possible memory
116 effect. The vials used for the standard preparation were cleaned following the same procedure adopted for
117 the ice samples. Considering the isobaric and polyatomic interferences affecting Fe, this element was
118 quantified using the interference-free isotope ⁵⁷Fe. External calibration curves with acidified standards (2%
119 HNO₃, Suprapure, Romil, UK) were prepared for Ca, Na and Fe from dilution of a certified single-element
120 1000 ppm ± 1% standard solution (Fisher Chemical, USA). The resulting R² for the external calibration
121 curves was 0.999 for all the elements. The Limit of Detection (LoD) for ⁵⁷Fe, calculated as three times the
122 standard deviation of the blank, was 0.8 µg L⁻¹. To assess accuracy for Fe, the TM-RAIN04 certified
123 reference material (National Research Council of Canada) was measured every 50 samples. The accuracy
124 was determined as a recovery percentage calculated as O/T %, where O is the determined value and T is the
125 certified value. For Fe, the accuracy was 104%, while precision, calculated as Relative Standard Deviation
126 (RSD %) of selected samples read multiple times (n = 5) during the analysis, was on average 5% (7% for
127 samples (n = 3) from the interglacial period, 4% for samples (n = 3) from the Last Glacial Period). For Ca
128 and Na, the LoD was 1 µg L⁻¹ and 3 µg L⁻¹, respectively. In the absence of a certified reference material, Ca
129 and Na accuracy was calculated using a Quality Control (QC) sample prepared at 10 µg L⁻¹ and measured
130 every 50 samples. Accuracy for Ca and Na, calculated as described above, was 94% and 108%, respectively,
131 while precision (RSD%) was on average 6% (4% for samples from the interglacial period and 7% for
132 samples from the Last Glacial Period) and 2% (for both periods), respectively.

133 nssCa concentration is commonly used as proxy for terrestrial inputs in polar regions and it is calculated
134 as $nssCa = [Ca] - ([Ca]/[Na])_{sw} \cdot [Na]$, where sw stays for seawater.

135

136

137 **3. Results and discussion**

138 **3.1 Fe fluxes from the NEEM core**

139 Fe and nssCa concentrations and fluxes were calculated as $F = C \cdot A$ (where F is the Fe flux, in mg m^{-2}
140 yr^{-1} , C is the Fe or nssCa concentration, in ng g^{-1} , and A the accumulation, in m yr^{-1} ice equivalent, whose
141 values are from Rasmussen et al., 2013). A pattern of higher dust (expressed as nssCa^{2+}) and Fe fluxes during
142 colder climate periods and lower dust and Fe fluxes during warmer climate periods is clearly recognizable
143 (Figure 2).

144 The Holocene (0.042 -11.7 kyr b2k) was characterized by average Fe fluxes of $0.5 \text{ mg m}^{-2} \text{ yr}^{-1}$ that
145 varied between $0.01 \text{ mg m}^{-2} \text{ yr}^{-1}$ and $5.3 \text{ mg m}^{-2} \text{ yr}^{-1}$ (Figure 2). The Coefficient of Variability (CV),
146 calculated as the ratio between the standard deviation and the mean value, was 1.2. The more recent 4000
147 years are characterized by the highest average Fe fluxes ($0.6 \pm 0.4 \text{ mg m}^{-2} \text{ yr}^{-1}$). The lowest Fe fluxes were
148 recorded between 4000 and 8000 years b2k ($0.3 \pm 0.2 \text{ mg m}^{-2} \text{ yr}^{-1}$). During the Younger Dryas (YD, 11.7 –
149 12.9 kyr b2k), an abrupt cooling was observed with a drop in the $\delta^{18}\text{O}$ value from -36.9‰ to -43.1‰.
150 Coincidentally, the recorded average Fe fluxes rise to $1.2 \pm 0.4 \text{ mg m}^{-2} \text{ yr}^{-1}$, higher than both the 12.9-13.9 kyr
151 b2k ($0.5 \pm 0.3 \text{ mg m}^{-2} \text{ yr}^{-1}$) and the 10.7- 11.7 kyr b2k ($0.3 \pm 0.2 \text{ mg m}^{-2} \text{ yr}^{-1}$) periods.

152 The Last Glacial Period (11.7-108 kyr b2k) showed Fe fluxes four-times higher ($2.0 \pm 2.2 \text{ mg m}^{-2} \text{ yr}^{-1}$)
153 than the Holocene, spanning from 0.05 to $16.5 \text{ mg m}^{-2} \text{ yr}^{-1}$ (Figure 2). However, a significant variability
154 during the Last Glacial Period was detected. During the LGM and MIS 4, average Fe fluxes were seven (3.6
155 $\pm 2.3 \text{ mg m}^{-2} \text{ yr}^{-1}$) and ten-times ($5.8 \pm 2.8 \text{ mg m}^{-2} \text{ yr}^{-1}$) greater than the Holocene average. Fe fluxes also
156 increased during the MIS 5c-MIS5b transition (87 kyr b2k), when a concurrent decrease in $\delta^{18}\text{O}$ values was
157 observed. During MIS 5c and MIS 5d, Fe fluxes were comparable with those detected during the Holocene.
158 The high frequency of the Dansgaard-Oeschger (D-O) events that characterized MIS 3 is mirrored by the
159 high variability in both nssCa and Fe fluxes. Each stadial period corresponded to an increase in both Fe and
160 nssCa. However, their variability was significantly different. During MIS 3, Fe fluxes showed maxima

161 values greater than $5 \text{ mg m}^{-2} \text{ yr}^{-1}$ during D-O 4, 9, 12, 15 (8.5, 6.5, 7.5, 6.6 $\text{mg m}^{-2} \text{ yr}^{-1}$ respectively), and
162 lower than $5 \text{ mg m}^{-2} \text{ yr}^{-1}$ during D-O 6, 7, 8, 10, 11 and 13 (3.9, 2.6, 4.1, 2.6, 2.7, 3.2 $\text{mg m}^{-2} \text{ yr}^{-1}$
163 respectively). This variability was significantly higher than the one recorded for nssCa, which showed
164 maxima values closer to $20 \text{ mg m}^{-2} \text{ yr}^{-1}$ for all the D-O events.

165 **3.2 Comparison with Fe fluxes from Antarctic ice cores**

166 The NEEM Fe ice core record allows the first comparison of Fe concentrations and fluxes between
167 the Arctic and Antarctica (Figure 3, Table 3). The only Antarctic Fe records that can reach at least the LGM
168 are from Talos Dome (TD) (Spolaor et al., 2013; Vallelonga et al., 2013), Law Dome (LD) (Edwards et al.,
169 2006; Edwards et al., 1998) and EPICA Dome C (EDC) (Wolff et al., 2006). However, we point out that
170 both the samples from Dome C and Talos Dome were acidified for at least 24 hours, leading to a possible
171 underestimation of the actual TDFe concentration. This implies that the general trends and features can be
172 comparable with the NEEM record, while absolute concentrations might differ due to the different
173 acidification procedure used (Koffman et al., 2014).

174 During the Holocene, in Antarctica, the average Fe flux and concentration values varied significantly
175 among the different sites with similar values recorded at the coastal sites (TD) and lower values in the
176 internal Antarctic Plateau (EDC) (Table 3). For TD, this was explained both through changes in atmospheric
177 transport patterns across Antarctica and through an additional local input of dust from proximal Antarctic
178 ice-free zones that affected coastal sites more than the central plateau, which was exclusively exposed to
179 remote sources such as southern South America (Albani et al., 2012; Delmonte et al., 2010b; Vallelonga et
180 al., 2013).

181 During the LGM, both TD and EDC shared a similar dust flux loading, comprised between 10 and 15 mg
182 $\text{m}^{-2} \text{ yr}^{-1}$ (Baccolo et al., 2018), and the same dust source region, as confirmed by the Sr-Nd isotopes
183 (Delmonte et al., 2010a). Compared to the Holocene, in TD the atmospheric dust fluxes increased of a factor
184 6, while in EDC the increase was approximately of a factor 25 (Delmonte et al., 2010b). This is mirrored by
185 a similar average Fe fluxes enhancement compared to the Holocene with values that were up to 4 and 21-fold
186 higher, respectively (Vallelonga et al., 2013; Wolff et al., 2006). The reason of these discrepancies is likely

187 due to the higher Holocene dust flux observed in TD compared to EDC, as a consequence of a relevant local
188 dust contribution at TD (Baccolo et al., 2018; Delmonte et al., 2010b).

189 During the Last Glacial Period, the most relevant dust source was the southern South America for both
190 TD and EDC (Basile et al., 1997; Delmonte et al., 2010b; Lambert et al., 2008). Dust fluxes peaked during
191 MIS 4 where both sites recorded maximum values around $10 \text{ mg m}^{-2} \text{ yr}^{-1}$ (Lambert et al., 2008; Vallelonga et
192 al., 2013) and comparable Fe fluxes ($0.17 \pm 0.07 \text{ mg m}^{-2} \text{ yr}^{-1}$ at TD and $0.12 \pm 0.07 \text{ mg m}^{-2} \text{ yr}^{-1}$ at EDC)
193 (Vallelonga et al., 2013; Wolff et al., 2006).

194 The LD record, due to the different analytical preparation of the samples, is not directly comparable with
195 TD and EDC. Nevertheless, we can still evaluate and discuss the Fe flux ratio between the Holocene and the
196 LGM. Unfortunately, for the LD record, there is no dust profile available, meaning that it is not possible to
197 assess which is the main dust and Fe sources to this location, although the Australian continent has been an
198 important source of mineral dust in the recent past (Edwards et al., 2006; Vallelonga et al., 2002). During the
199 LGM, Fe fluxes increased 10-fold compared to the Holocene period, 2.5 times more than what was observed
200 in TD. Similarly to what observed in the EDC record, this difference might be explained either by the
201 absence of local dust sources that affected LD during the Holocene, or by the lower sampling frequency for
202 the LD record ($n = 27$) compared to TD ($n = 801$).

203 Despite the different acidification times, the overall picture during the Holocene is that the average Fe
204 fluxes in NEEM ($0.5 \text{ mg m}^{-2} \text{ yr}^{-1}$, $\text{CV} = 1.2$) were higher than in Antarctica. Among the Antarctic Fe fluxes,
205 TD ($0.09 \text{ mg m}^{-2} \text{ yr}^{-1}$, $\text{CV} = 1.2$) and LD ($0.04 \text{ mg m}^{-2} \text{ yr}^{-1}$, $\text{CV} = 0.5$) were higher than the ones recorded at
206 EDC ($0.007 \text{ mg m}^{-2} \text{ yr}^{-1}$, $\text{CV} = 0.2$).

207 In NEEM, the LGM (19 – 26.5 kyr b2k) was characterized by a 10-fold and 7-fold enhancement in dust
208 (expressed as nssCa) and Fe fluxes, respectively. A similar behaviour was observed in the Antarctic cores as
209 described above (Table 3). Considering that the atmospheric CO_2 concentration dropped down to 180 ppm
210 (Köhler et al., 2017), the global Fe fluxes enhancement likely contributed to part of this decrease, promoting
211 marine productivity in some HNLC regions (Amo and Minagawa, 2003; Kawahata et al., 2000; Martínez-
212 García et al., 2011).

213 MIS 4 (60-71 kyr b2k) NEEM Fe fluxes were higher compared to all the other investigated records.
214 Compared to the LGM average, during MIS 4, dust (Ruth, 2007), nssCa and Fe fluxes (this work) in the
215 Arctic exhibited a ≈ 1.5 -fold increase (Table 3), while they were lower both in TD and EDC. To explain this
216 behaviour we suggest some hypotheses. The first is that the increase in dust and Fe fluxes can be attributable
217 to changes in the atmospheric circulation, likely due to the topographic influence of the Laurentide Ice Sheet
218 (LIS). Indeed, during the LGM, LIS was nearly 2 times larger than at MIS 4 (Löffverström et al., 2014;
219 Tulenko et al., 2020) and it might have caused a stronger meridional splitting of the westerlies (Löffverström
220 et al., 2014) and a southward migration of their mean position (Kang et al., 2015; Manabe and Broccoli,
221 1985). The southward shift during the LGM might have produced a reduction of strong winds passing over
222 the source areas (i.e. Taklimakan and Gobi deserts) (Kang et al., 2015) and/or a stronger southward Fe and
223 dust deposition over the Chinese Loess Plateau (Zhang et al., 2014) and the mid-latitude North Pacific (Sun
224 et al., 2018). In contrast, during MIS 4, the westerlies might have been located northward (i.e. over the
225 Taklimakan and Gobi deserts) and characterized by a less marked meridional splitting (Löffverström et al.,
226 2014), conveying a larger amount of dust to Greenland. We also propose two alternative hypotheses that rely
227 on 1) the possibility that additional dust sources (e.g. Saharan dust) might have reached Greenland during
228 MIS 4, and 2) that during MIS 4, the Asian monsoon system was stronger in winter than in summer,
229 producing drier conditions that caused an enhanced dust production and transport to Greenland (Xiao et al.,
230 1999). However, to better address this point, a more comprehensive investigation that involves a large set of
231 palaeorecords and atmospheric modelling is required and it is beyond the scopes of the manuscript.

232 **3.3 Comparison with lower-resolution Fe NEEM measurements**

233 A parallel study that reported Fe concentration from the NEEM ice core was published (Xiao et al.,
234 2020). It reports the TDFe and DFe concentration and fluxes with a lower temporal resolution ($n = 166$) than
235 the current investigation ($n = 1596$). Moreover, the analytical approach was different since the melted ice
236 samples were filtered at $0.45 \mu\text{m}$ and acidified for six weeks before the analysis. Even though the overall
237 pattern between the two records is similar, we observe at least two critical differences. The first is that the
238 average Fe concentration in Xiao et al 2020 is 4-fold higher than the one found in our study (101.4 ng g^{-1} vs
239 20.4 ng g^{-1}) as well as the Fe concentration range ($1.5\text{-}1194.5 \text{ ng g}^{-1}$ vs $>\text{LoD} - 457.6 \text{ ng g}^{-1}$ in our
240 investigation). These differences are also reflected in the average Fe fluxes, which are $1.2 \text{ mg m}^{-2} \text{ yr}^{-1}$ (0.5

241 $\text{mg m}^{-2} \text{yr}^{-1}$ in this study) for the Holocene and $12.5 \text{ mg m}^{-2} \text{yr}^{-1}$ for the LGM ($3.6 \text{ mg m}^{-2} \text{yr}^{-1}$ in this study).
242 Moreover, the LGM Fe flux increase compared to the Holocene is 10-fold, while we found a 7-fold
243 enhancement.

244 The second difference between the two analyses arises when comparing MIS 4 average fluxes and
245 concentrations. Our record shows a 1.5 increase with respect to the LGM, consistently with a similar
246 enhancement of nssCa and dust (Ruth, 2007). This behavior was not mirrored in the other study where TDFe
247 was higher during the LGM than MIS 4. Possible reasons might rely on the different temporal resolution and
248 on the discrepancies between the adopted analytical approaches that highlight the need to standardize the
249 analytical procedures when trace elements are analysed in ice and snow samples in order to have a more
250 reliable comparison among both different and identical locations.

251 **3.4 Fe and marine productivity in the Northern Hemisphere**

252 Considering the biological relevance of Fe and taking advantage from the Fe flux record retrieved from
253 the NEEM ice core, one important question remains regarding whether its flux increase during the Last
254 Glacial Period triggered the marine productivity in the HNLC region of the North Pacific (Olgun et al.,
255 2011).

256 Nowadays, a significant amount of Asian dust (250 Mt yr^{-1}) is primarily deposited over the HNLC region
257 of the subarctic Pacific (Serno et al., 2014; Zhang et al., 2003) and the marine productivity changes in this
258 oceanic region might reflect potential Fe fertilization effects promoted by atmospheric Fe supply. During
259 modern times, both increases in aeolian influx from Asia (Young et al., 1991) and sporadic Fe input from
260 volcanic eruptions (Langmann et al., 2010) resulted in enhanced MPP by more than 60%. Moreover, recent
261 Fe-fertilization experiments performed south of the Gulf of Alaska (McDonald et al., 1999; Tsuda et al.,
262 2003), showed significant increases in the abundance of diatoms and in chlorophyll-a concentration (Boyd et
263 al., 1996), indicating that the North Pacific is maybe sensitive to atmospheric Fe inputs. However, no data
264 are available to evaluate if the Fe-sensitivity of the subarctic Pacific Ocean holds even over longer timescales
265 and, if an increase in the aeolian Fe supply, observed during glacial periods, could explain the MPP
266 variability in the subarctic Pacific Ocean. To address this point, we compared the NEEM Fe record with
267 different marine sediment cores (Table 4).

268 Previous geochemical evidence indicates that for both interglacial and glacial periods the dust
269 source influencing Greenland and the North Pacific mainly originated from the East Asian deserts
270 (Schüpbach et al., 2018; Serno et al., 2014). However, considering that there are no aeolian Fe flux records
271 from the marine sediment cores, they might have received different amount of Fe compared to what observed
272 in the ice core record. Through a comparison between a marine sediment record from the western Subarctic
273 Pacific Ocean (SO202-07-6) and the NGRIP ice core, it has been shown that dust fluxes changed coherently
274 and simultaneously during abrupt climate changes, even though with different amplitude (Serno et al., 2015).
275 The larger variability observed in NGRIP, as well as in NEEM, than in marine sediments, indicates changes
276 in the atmospheric dust transport from the source areas to Greenland (e.g. rate of aerosol rainout, different
277 wind strength...).

278 Recently, it has been proposed that additional dust sources might have influenced Greenland in the
279 last 31 kyrs (Han et al., 2018; Lupker et al., 2010). Based on the Sr and Pb isotopes quantification, it was
280 highlighted that the Saharan dust contributed to the overall NEEM dust budget mainly during the Younger
281 Dryas (12-73%) and between 17 kyrs and 22 kyrs (16-70%), while the Taklimakan and Gobi contribution
282 (i.e. eastern Asia sources) was dominant (55-94%) prior to 22 kyrs (Han et al., 2018). Accordingly with the
283 available literature (Svensson et al., 2000), we assume that despite this secondary source, the main dust
284 source for the NEEM ice core during the Last Glacial Period is still represented by the Gobi and Taklimakan
285 deserts. This is also coherent with the dust changes synchronicity among Greenland, the Chinese loess (Ruth
286 et al., 2007) and the northern Pacific sediment records located downwind of the Asian dust sources
287 (Schüpbach et al., 2018; Serno et al., 2015). However, additional investigations are needed to assess the
288 magnitude of the Saharan dust contribution prior to 31 kyrs.

289 All considered (i.e. different dust amplitude and other potential dust sources), and observing that the
290 overall pattern of higher dust deposition during the coldest periods is consistent between the ice and
291 sediment core records, we assumed that the Fe flux changes observed in NEEM are representative for the
292 aeolian Fe supply to the subarctic Pacific Ocean.

293 To evaluate whether past marine productivity was influenced by atmospheric Fe supply for the
294 period ranging from the LGM to the Holocene, we compared the NEEM record with the high temporal

295 resolution SO202-27-6 (from the Patton-Murray Rise plateau, eastern subarctic Pacific Ocean) and the
296 SO202-07-6 (from the Detroit Seamount, western subarctic Pacific Ocean) productivity records (Méheust et
297 al., 2018). For a long-term record, we relied on the ODP887 (McDonald et al., 1999) and the ODP882 (Haug
298 et al., 1995) sediment cores, located close to SO202-27-6 and SO202-07-6, respectively. A comparison over
299 the last 108 kyr between the NEEM record and the S-2 sediment core (from the Shatsky Rise, mid-latitude
300 North Pacific) was also performed (Amo and Minagawa, 2003) (Figure 4, Table 4).

301 The past marine primary productivity reconstruction was performed relying on the Si/Al ratio, % of
302 biogenic silica and brassicasterol concentration. Si/Al ratio is used as a proxy for opal, or biogenic silica
303 (diatoms), in the absence of directly measured opal concentrations. The normalization to Al removes any
304 possible variable inputs of lithogenic detritus (McDonald et al., 1999). Brassicasterol is a sterol compound
305 which has been used as a molecular indicator of the presence of diatoms (Sachs and Anderson, 2005).
306 Brassicasterol concentration is also used, together with highly branched isoprenoid alkenes (IP₂₅), for the
307 PIP₂₅ calculation, which is a proxy for the evaluation of past sea-ice conditions (Méheust et al., 2018; Müller
308 et al., 2011)

309 3.4.1 From the LGM to the Holocene

310 During the Last Glacial Maximum, the Fe fluxes recorded in the NEEM ice core were 7 times higher
311 compared to the Holocene. However, marine productivity in the subarctic Pacific Ocean, expressed as Si/Al
312 ratio (McDonald et al., 1999), % biogenic silica (Haug et al., 1995) and brassicasterol concentration
313 (Méheust et al., 2018), was at its lowest level (Figures 4, 5). Reconstructions based on the foraminifera-
314 bound $\delta^{15}\text{N}$ (FB- $\delta^{15}\text{N}$), a proxy which indicates the degree of nitrate consumption by phytoplankton
315 (Martínez-García et al., 2014), showed that, in the western subarctic Pacific Ocean, the nitrate consumption
316 was more complete during the LGM and the YD (i.e. when MPP was low) compared to the warmest periods
317 (Ren et al., 2015). In other words, during the coldest and dustiest periods, the nitrate consumption efficiency
318 was higher (i.e. increase in the FB- $\delta^{15}\text{N}$ values) than during the interglacials, even though MPP was low.
319 This apparent contradiction can be explained by an increase in water stratification (either by reduced
320 upwelling or vertical mixing), where the most nutrient-rich and oxygen depleted waters were shifted to
321 deeper depths, while nutrient-depleted and better-ventilated waters rested above a hydrographic boundary at

322 1500-2000 m (Kohfeld and Chase, 2017). Water stratification led to minimal input of nutrients to the surface
323 ocean, leading the system towards a major nutrient limitation (Kienast et al., 2004; Ren et al., 2015). Among
324 the several possible reasons that can explain the increase in water stratification in the Glacial North Pacific,
325 we report two hypotheses. The first relies on the glacial closure of the Bering Strait that reduced the
326 freshwater export from the Pacific Ocean to the Atlantic, retaining more freshwater in the North Pacific
327 (Talley, 2008). The second involves sea-ice formation. When sea-ice forms, in the Okhotsk and Bering Seas,
328 brine rejection occurs, increasing water density and creating the more saline and denser North Pacific
329 Intermediate Water (NPIW). When the wind blows the sea-ice away from where it was originally formed,
330 brine rejection can further proceed at the same location following the formation of new sea-ice. The
331 continuous brine rejection promotes the freshening of surface waters and strengthens water stratification
332 (Costa et al., 2018).

333 An additional explanation for the observed lower productivity during glacial periods arises from the
334 higher extent of perennial sea-ice that might have played a role in creating a physical barrier between the
335 atmosphere and the marine environment, reducing the amount of available sunlight and the **direct** deposition
336 of bioavailable Fe **on the seawater surface** (Kienast et al., 2004; Méheust et al., 2018). Marine sediment
337 records, collected in the eastern and western subarctic Pacific and in the Bering Sea, showed extended spring
338 ice-cover during the LGM (Méheust et al., 2018; Méheust et al., 2016) when the Fe fluxes were at their
339 maxima. The progressive decrease in perennial sea-ice coverage recorded after the LGM led to an increase in
340 the marine productivity (Figure 5), with a maximum during the Bølling-Allerød (B/A) warm event (\approx 13-15
341 kyr ago). The possible relevance of sea-ice in modulating MPP at the highest latitude of the Pacific Ocean
342 during the LGM is strengthened by a marine sediment record collected in the **mid-latitude North Pacific**
343 (Amo and Minagawa, 2003), which, because of its southernmost location, did not experience any sea-ice
344 condition. During the LGM, contrarily to what is observed in the subarctic Pacific, a prominent maximum in
345 marine productivity was recorded, suggesting that Fe could have triggered an important phytoplankton
346 response (Figure 4d). The Fe-sensitivity of the **mid-latitude North Pacific** is confirmed during the Holocene,
347 when the Fe fluxes were at their minima and the productivity, expressed as MAR (Mass Accumulation Rate)
348 C_{37} alkenone ($\mu\text{g cm}^{-2} \text{ kyr}^{-1}$), was at its lowest level. **A plausible explanation is that stratified waters did not**
349 **characterize this region during the Last Glacial Period** and thus it was not affected by the limitation of major

350 nutrients. Unfortunately, neither FB- $\delta^{15}\text{N}$ nor information about water stratification are available for this
351 record.

352 However, there might be other reasons that could explain the strengthening in MPP during the B/A
353 warm period. Among them, we propose the increase in the sea-level that inundated previously exposed lands
354 which might have entrained iron and other nutrients to the marine ecosystem (Davies et al., 2011), or
355 changes in the oceanic circulation (McManus et al., 2004). Indeed, at the onset of the B/A event, the
356 meridional overturning circulation rapidly accelerated and this might have produced an upward displacement
357 of the nutrient-rich North Pacific Deep Waters towards intermediate depths, promoting an injection of
358 nutrients to surface waters which resulted in an enhanced productivity.

359 These additional explanations shed light on the marginal role that atmospheric Fe fertilization had in
360 promoting MPP in the subarctic Pacific Ocean since other players had a more significant role (Kohfeld and
361 Chase, 2017).

362 **3.4.2 From 108 kyr to the LGM**

363 According to the available records, marine productivity changed heterogeneously in the Pacific
364 Ocean during the Last Glacial Period (Figure 4).

365 It is challenging to state, with a high degree of confidence, whether Fe-fertilization triggered a
366 phytoplankton bloom or not in the HNLC subarctic North Pacific. This is due to the different responses that
367 the western and the eastern side of the subarctic North Pacific showed with respect to the atmospheric Fe
368 supply (Figure 4). In the eastern subarctic Pacific, the increase in the aeolian Fe fluxes was mirrored by a
369 phytoplankton response during the MIS 5.2 and the MIS 5 / MIS 4 transition. The subsequent decrease in
370 MPP during the MIS 4 suggests that the prolonged Fe supply during the coldest stadial might have led the
371 ecosystem towards the limitation of other nutrients (Kienast et al., 2014) following the same mechanisms
372 described in the previous section. The enhanced water stratification during those periods, as suggested by
373 stable oxygen isotope ratios in planktonic foraminifera (Zahn et al., 1991), did not allow a supply of
374 macronutrients from below the mixed layer. Thus, additional atmospheric Fe supply had little effect on
375 phytoplankton productivity, suggesting their growth was likely limited by the lack of major nutrients
376 (Kienast et al., 2004). In the western subarctic Pacific, the increase in productivity was recorded also in

377 periods with low atmospheric Fe fluxes (e.g. from 100 to 90 kyr at ODP882), strengthening the hypothesis
378 that other **influences** (e.g. meltwater inputs, continental margin supply, sea-ice) had a more relevant role
379 (Kienast et al., 2004; Lam and Bishop, 2008) **than atmospheric Fe supply**.

380 On the contrary to what was observed in the subarctic Pacific, the S-2 sediment core collected in the
381 **mid-latitude North Pacific** (Amo and Minagawa, 2003), showed a marked increase in primary productivity
382 during MIS 4 and the overall Last Glacial Period when the Fe fluxes were higher (Figure 4). MPP in the **mid-**
383 **latitude North Pacific might have been more sensitive** to the atmospheric Fe supply, suggesting that the high
384 degree of upper ocean stratification that characterized the subarctic region of the Pacific Ocean did not likely
385 affect the **mid-latitude North Pacific allowing for a continuous supply of macronutrients**. The observed
386 **increase in dust transport (and Fe deposition) could have then stimulated marine productivity** (Kienast et al.,
387 **2004**).

388 **4. Conclusions and future perspectives**

389 In this study, we provided the first Fe record **from mineral dust input** retrieved from the NEEM ice core.
390 Through the comparison with other available Fe records, we observed that Fe fluxes were higher in
391 Greenland than in Antarctica. The greatest difference observed between the sites in opposite hemispheres
392 occurred during MIS4, when Fe fluxes in NEEM **were 1.5 times higher than during the LGM, while, in TD**
393 **and EDC, were lower**. To explain this behaviour, we advanced two hypotheses (i.e. **change in the**
394 **atmospheric circulation or additional dust sources that reached Greenland**), even though more detailed
395 **investigations are needed**.

396 Merging our record with marine productivity data, we found that a link between Fe transport and ocean
397 productivity holds in the **mid-latitude North Pacific, indicating that this area might be sensitive to the**
398 **atmospheric Fe supply**. On the contrary, in the subarctic Pacific, we did not find any overwhelming evidence
399 that the increase in the atmospheric Fe fluxes triggered a phytoplankton response. This indicates that other
400 players, such as sea-ice and increased water stratification during the coldest periods had a more relevant role
401 in modulating the MPP in the HNLC region of the North Pacific on a millennial time scale.

402 This study provides an upper limit for estimating the potentially bioavailable Fe supplied to marine
403 phytoplankton in the North Pacific region, however additional studies should focus on analysing the labile
404 and bioavailable Fe fractions to constrain realistic Fe supply and response of the marine ecosystem.

405 **Data availability**

406 Data will be published on Pangaea

407 **Author contributions**

408 FB wrote the manuscript. FB, AS and CB designed the research. JG, CT and GC performed the analyses. PV
409 contributed to the interpretation of the results.

410 **Competing interests**

411 The authors declare that they have no conflict of interest.

412 **Acknowledgments**

413 We sincerely thank all the persons involved in the logistics, drilling operations, ice-core processing and
414 sample collection. NEEM is directed and organized by the Center of Ice and Climate at the Niels Bohr
415 Institute and US NSF Office of Polar Programs and it is supported by funding agencies and institutions in
416 Belgium (FNRS-CFB and FWO), Canada (NRCan/GSC), China (CAS), Denmark (FIST), France (IPEV,
417 CNRS/INSU, CEA and ANR), Germany (AWI), Iceland (RannIs), Japan (NIPR), Korea (KOPRI), The
418 Netherlands (NWO/ALW), Sweden (VR), Switzerland (SNF), United Kingdom (NERC), and the USA (US
419 NSF, Office of Polar Programs).

420

421 **Figures and tables**

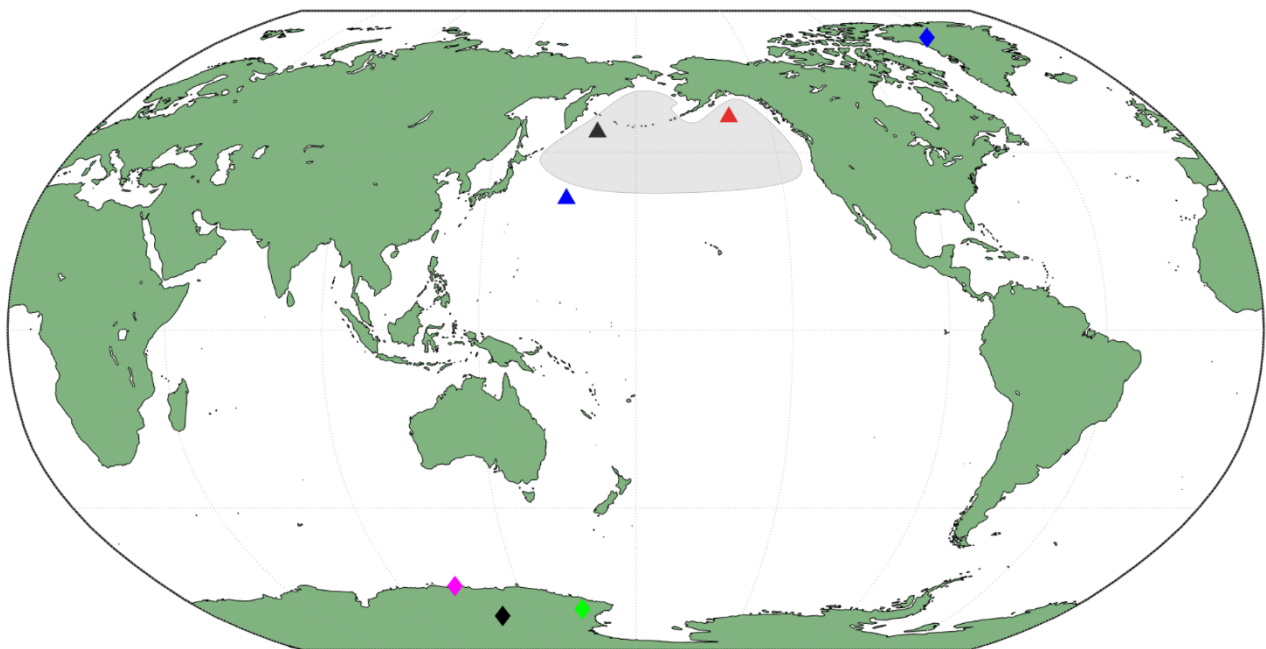
422

423 **Figure 1** - Locations of the NEEM ice core (blue diamond, this study), the LD ice core (pink triangle,
424 Edwards et al., 2006), EDC ice core (black diamond, Wolff et al., 2006) and TD ice core (green diamond,
425 Vallelonga et al., 2013). We retrieved palaeoproductivity data for the eastern North Pacific (black triangle)
426 from the ODP882 (Haug et al., 1995) and SO202-27-6 (Méheust et al., 2018) sediments cores, while for the
427 western Pacific Ocean (red triangle) from the ODP887 (McDonald et al., 1999) and SO202-07-6 (Méheust et
428 al., 2018) sediment cores. The palaeoproductivity record from the mid-latitude North Pacific was retrieved
429 from the S-2 sediment core (blue triangle, Amo and Minagawa, 2003).

430

431

432



433

434

435

436

437

438

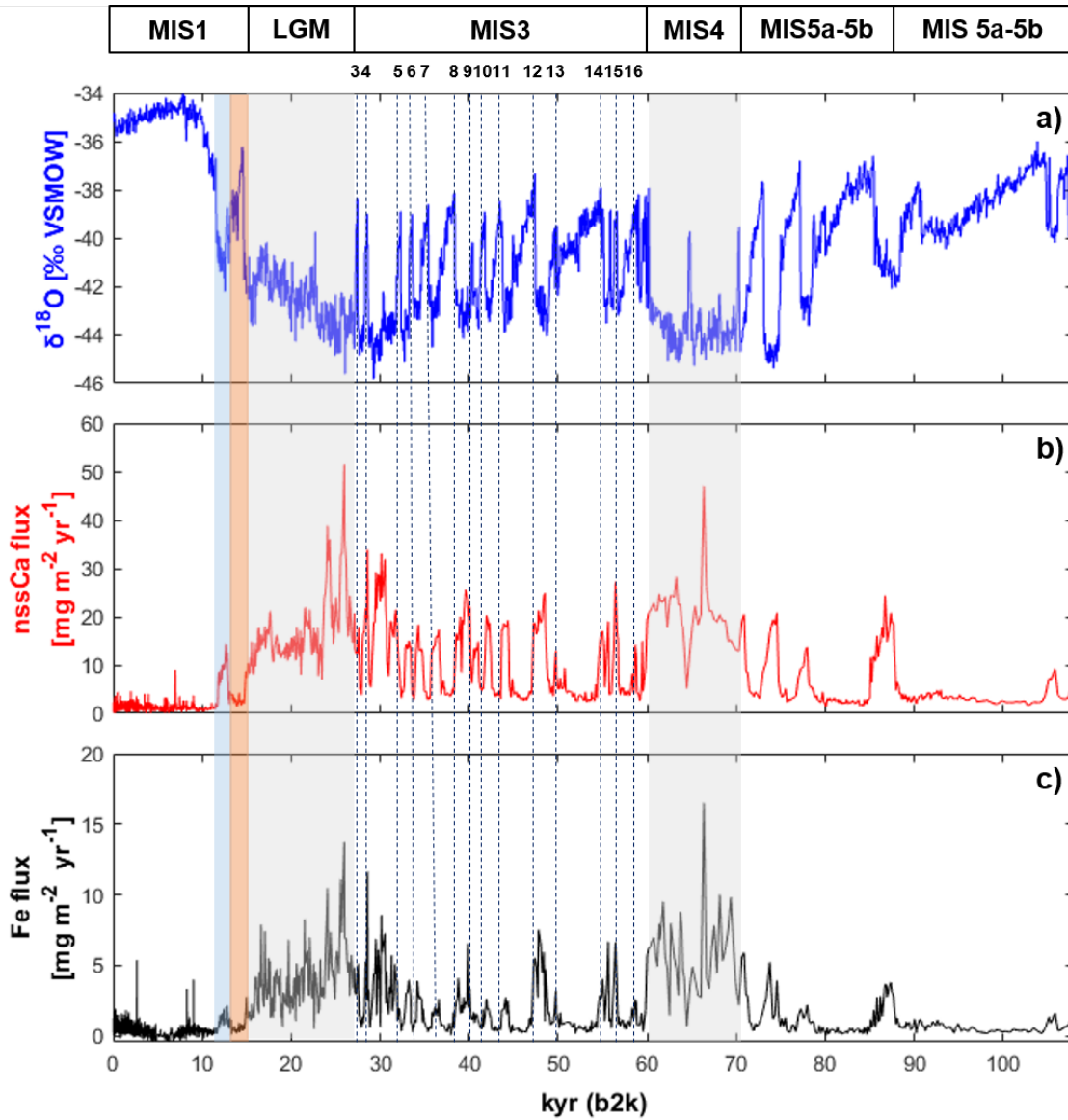
439

440

441

442 **Figure 2** – Panel a) $\delta^{18}\text{O}$ (blue line) profile is from the NGRIP ice core (North Greenland Ice Core Project,
 443 2007). Panel b) *nssCa* flux (red line) from the NEEM ice core. Panel c) and Fe flux (black line) from the
 444 NEEM ice core. Shaded blue rectangle: Younger Dryas. Shaded orange rectangle: Bølling-Allerød. Numbers
 445 in the upper panel indicate the Dansgaard-Oeschger events from 3 to 16.

446



447

448

449

450

451

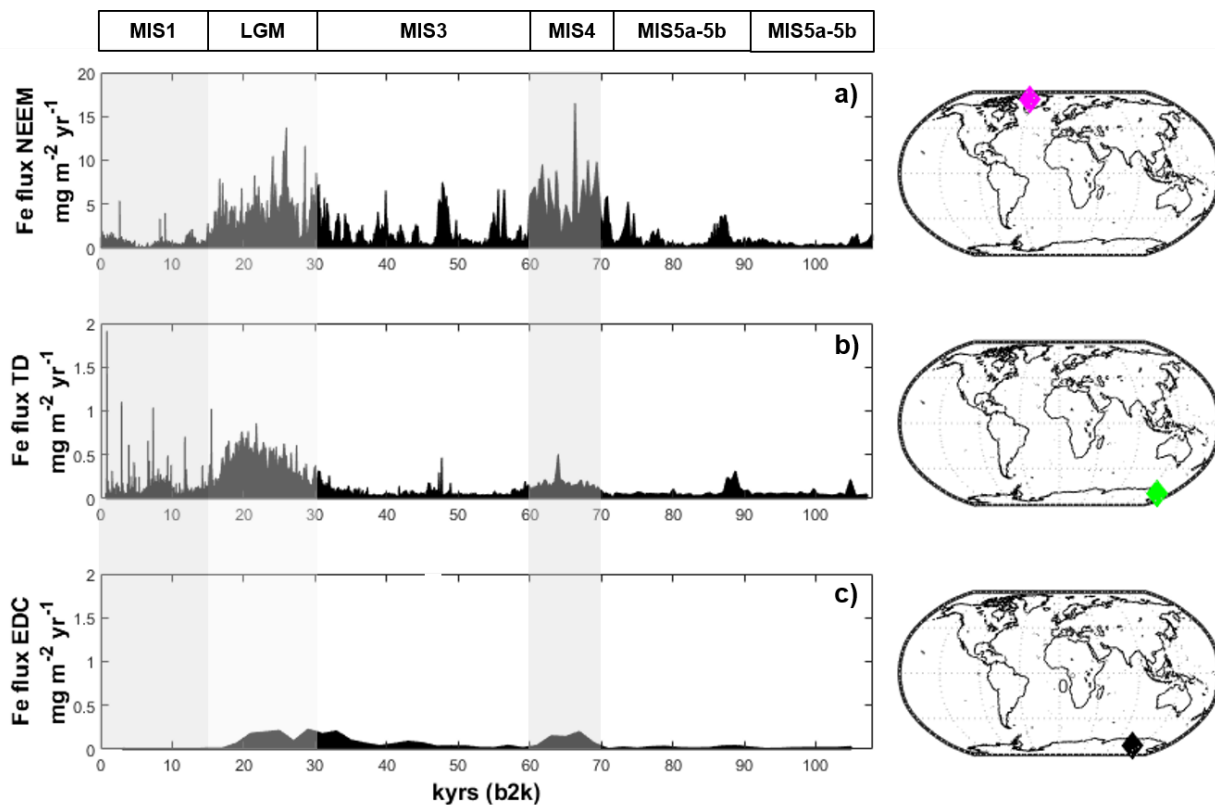
452

453

454 **Figure 3** – Comparison of the Fe fluxes among a) NEEM (this work, pink diamond), b) TD (Vallelonga et
455 al., 2013; green diamond) and c) EDC (Wolff et al., 2006; black diamond). Note that the y-axis for NEEM
456 ranges from 0 to 20 $\text{mg m}^{-2} \text{yr}^{-1}$, while the y-axis for TD and EDC ranges from 0 to 2 $\text{mg m}^{-2} \text{yr}^{-1}$.

457

458



459

460

461

462

463

464

465

466

467

468

469

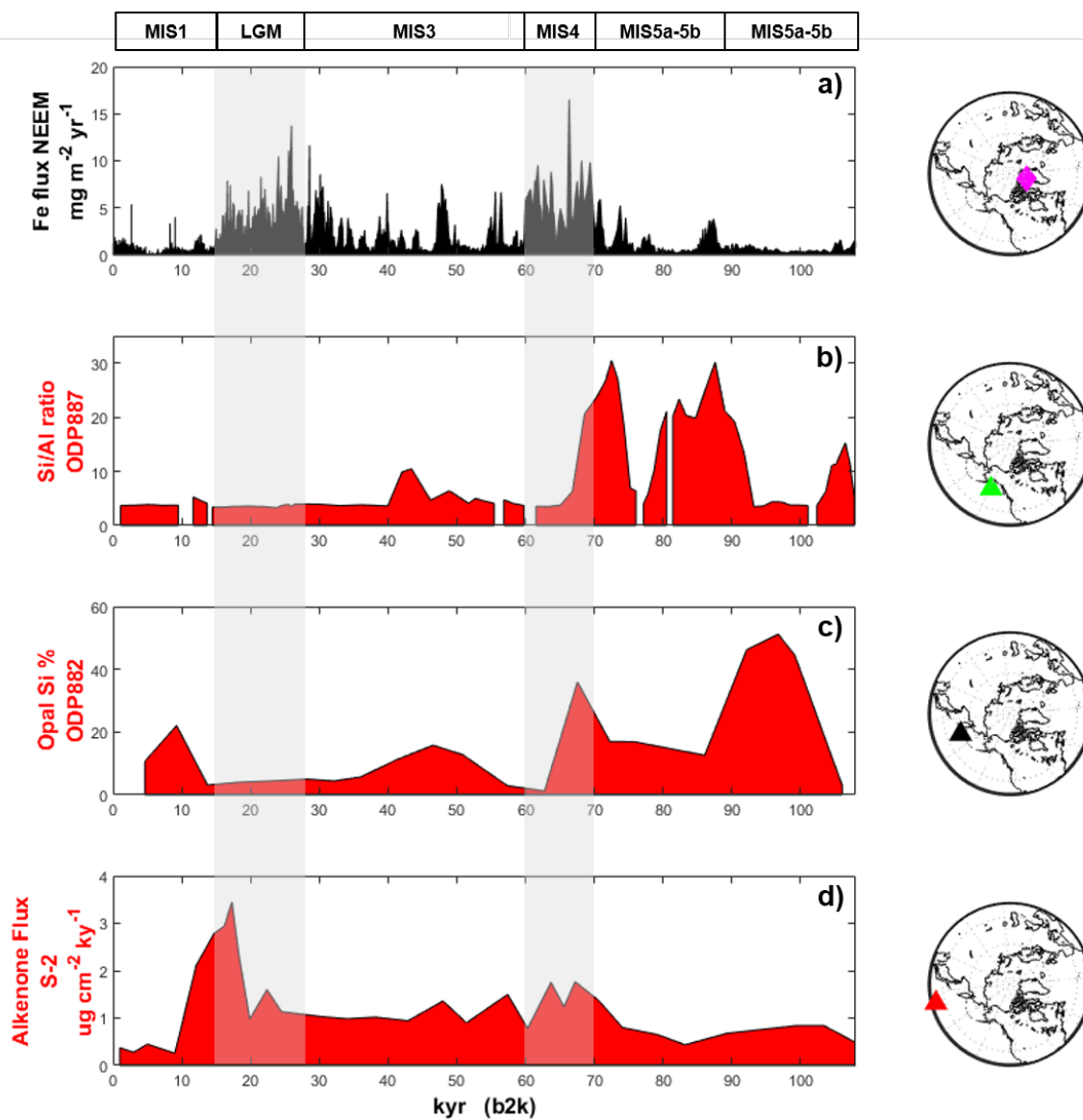
470

471

472

473 **Figure 4** – Comparison between Fe fluxes (black line, panel a) from NEEM (this work; pink diamond), with
 474 marine productivity (red line, panel b) from ODP887, eastern subarctic Pacific (McDonald et al., 1999; green
 475 triangle), ODP882 (red line, panel c), western subarctic Pacific (Haug et al., 1995; black triangle) and S-2
 476 (red line, panel d), **mid-latitude North Pacific** (Amo and Minagawa, 2003; red triangle). Due to their limited
 477 temporal extension, productivity records from SO202-07-6 and SO202-07-26 are not discussed in this figure,
 478 but in Figure 4.

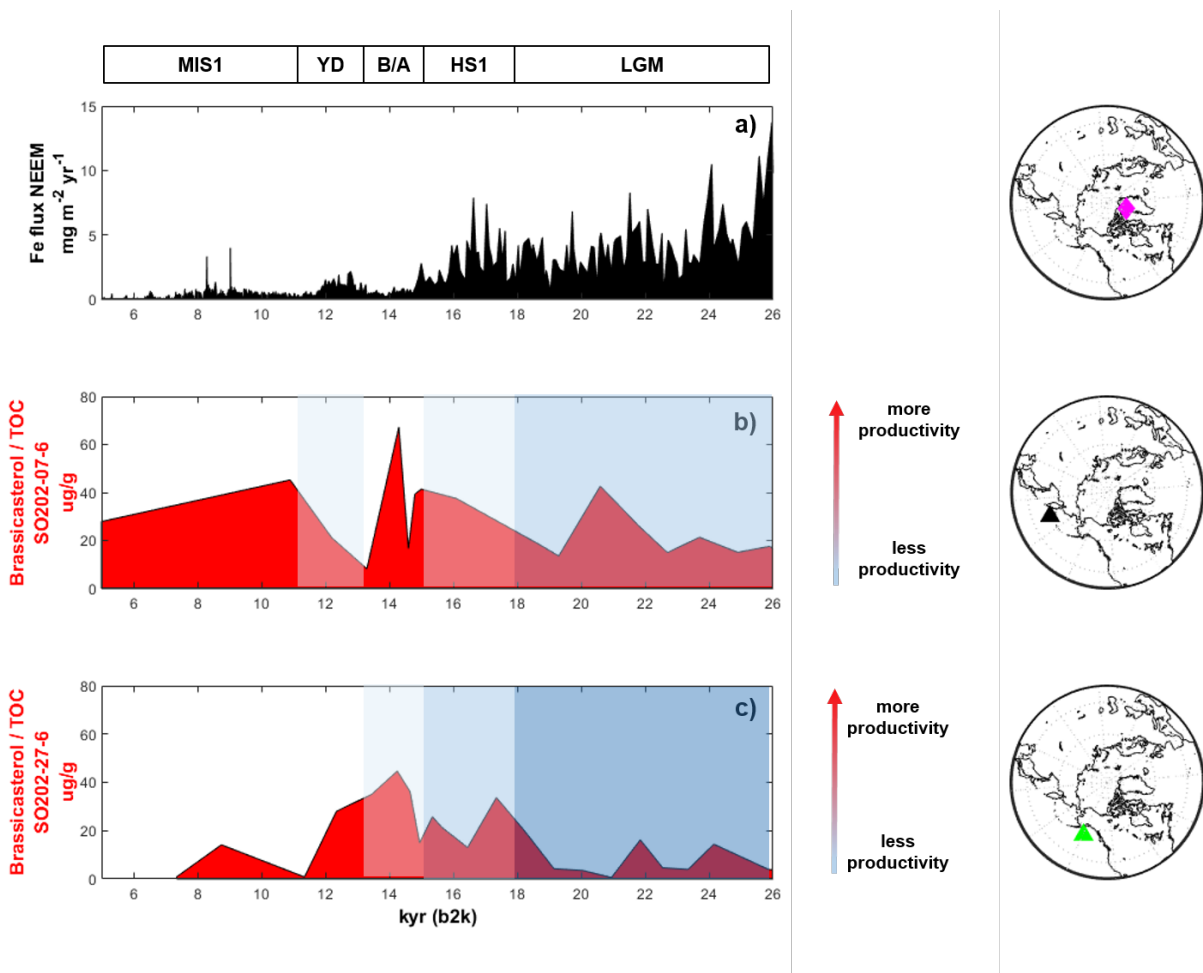
479



480

481 **Figure 5** – Relationship between Fe flux in the NEEM core, and MPP in subarctic Pacific Ocean over the
 482 last 26 kyr, where higher brassicasterol-total organic carbon ratio represents an increase in productivity. Sea-
 483 ice data are from Meheust et al. (2018): prevalently extended sea-ice (dark blue rectangle), prevalently
 484 marginal sea-ice (blue rectangle), prevalently variable sea-ice (light blue rectangle), prevalently ice-free
 485 (white rectangle). Fe flux record (black line, panel a), productivity in the eastern subarctic Pacific Ocean
 486 (SO202-07-6, red line, panel b) and productivity in the western subarctic Pacific Ocean (S0202-27-6, red
 487 line, panel c). Productivity pulses were recorded when sea-ice changed its conditions towards ice-free
 488 conditions. YD = Younger Dryas, B/A = Bolling-Allerod event, HS1 = Heinrich Stadial 1, LGM = Last
 489 Glacial Maximum.

490



491

492

493

494

495

496

497 **Table 1 - Temporal resolution of NEEM ice core, accordingly with the GICC05modelext-NEEM-1 age scale**
 498 **(Rasmussen et al., 2013).** Ice samples for ICP-MS analysis were collected with a resolution of 110 cm.

499

Temporal resolution	Period
10 years	Holocene (present-7.2 kyr)
22 years	Holocene (7.2 kyr-LGM)
110 years	Last Glacial Maximum
73 years	Interstadials
147 years	28-59 kyr
440 years	59-70 kyr
220 years	70-96 kyr
730 years	96-110 kyr

500

501

502

503 **Table 2 – Fe and nssCa average concentration (ng g⁻¹) and fluxes (mg m⁻² yr⁻¹) from the NEEM ice core.**
 504 **More details in the text. The Coefficient of Variability (CV) was calculated for Fe and nssCa fluxes and it is**
 505 **reported in bold.**

	Fe average concentration /ng g ⁻¹	Fe average fluxes /mg m ⁻² yr ⁻¹	nssCa average concentration /ng g ⁻¹	nssCa average fluxes /mg m ⁻² yr ⁻¹
Holocene (0.042 -11.7 kyr b2k)	2.9	0.5 (CV 1.2)	7.2	1.4 (CV 2.3)
Glacial (11.7– 108 kyr b2k)	44.3	2.0 (CV 1.1)	210.8	10.0 (CV 0.8)
Younger Dryas (11.7 – 12.9 kyr b2k)	18.2	1.2 (CV 0.3)	135.2	8.5 (CV 0.4)
LGM (14.5 – 26.5 kyr b2k)	86.3	3.6 (CV 0.6)	273.3	12.3 (CV 0.7)
MIS 3 (26.5 – 60 kyr b2k)	45.5	1.9 (CV 1.0)	216.6	10.2 (CV 0.8)
MIS 4 (60 - 71 kyr b2k)	146.4	5.8 (CV 0.5)	510.2	20.5 (CV 0.3)
MIS 5a-MIS 5b (71-87 kyr b2k)	17.0	1.1 (CV 1.0)	98.6	6.3 (CV 0.8)
MIS 5c-MIS 5d (87-108 kyr b2k)	6.5	0.8 (CV 0.8)	50.4	4.3 (CV 0.9)

506

507

508

509

510

511 **Table 3** – Comparison of average Fe concentration ([Fe] in ng g⁻¹) and fluxes (in mg m⁻² yr⁻¹) among four
512 different ice cores: NEEM, Talos Dome (Vallelonga et al., 2013), Law Dome (Edwards et al., 2006) and
513 Dome C (Wolff et al., 2006). n.a. = not available. Average Fe concentration at DC is not available since the
514 accumulation rate at that site during MIS4 is unavailable. Data from Law Dome spans from 59 to 8.5 b2k
515 (for the Holocene) and from 18.2 to 23.7 b2k (for the LGM). The Coefficient of Variability (CV) was
516 calculated for Fe fluxes and it is reported in bold for all the cores.

517

	Greenland		Antarctica					
	NEEM		Talos Dome		Law Dome		Dome C	
	[Fe] /ng g ⁻¹	Fe flux /mg m ⁻² yr ⁻¹	[Fe] /ng g ⁻¹	Fe flux /mg m ⁻² yr ⁻¹	[Fe] /ng g ⁻¹	Fe flux /mg m ⁻² yr ⁻¹	[Fe] /ng g ⁻¹	Fe flux /mg m ⁻² yr ⁻¹
Holocene (0.042 -11.7 kyr b2k)	2.9	0.5 (CV 1.2)	1.4	0.09 (CV 1.2)	0.09	0.04 (CV 0.5)	0.2	0.007 (CV 0.2)
LGM (14.5 -26.5 kyr b2k)	86.3	3.6 (CV 0.6)	10.3	0.4 (CV 0.5)	2.4	0.4 (CV 0.7)	16	0.15 (CV 0.5)
MIS4 (60- 71 kyr b2k)	146.4	5.8 (CV 0.5)	3.1	0.17 (CV 0.4)	n.a.	n.a.	n.a.	0.12 (CV 0.6)
LGM/Holocene ratio	30	7	7	4	27	10	80	21
MIS4/LGM ratio	1.7	1.5	0.3	0.4	n.a.	n.a.	n.a.	0.8

518

519

520 **Table 4** – Summary of locations and data source for all the cores (both ice and sediment cores) discussed in
521 the text (NH = Northern Hemisphere; SH = Southern Hemisphere)

Name	Core	Location	Reference	Latitude/Longitude
NEEM ice	Ice core	NH	<i>This work</i>	77°45'N, 51°06'W
Talos Dome	Ice core	SH	Vallelonga et al., 2013	73°0'S 158°0'E
Law Dome	Ice core	SH	Edwards et al., 2006	66°46'S 112°48'E
Dome C	Ice core	SH	Wolff et al., 2006	75°06'S; 123°23' E
ODP882	Marine sediment	NH	Haug et al., 1995	50°22'N; 167°36'E
ODP887	Marine sediment	NH	McDonald et al., 1999	54°22'N; 148°27'W
SO202-27-6	Marine sediment	NH	Meheust et al., 2018	54°12'N; 149°36'W
SO202-07-6	Marine sediment	NH	Meheust et al., 2018	51°16'N; 167°42'E
S-2	Marine sediment	NH	Amo and Minagawa, 2003	33°22'N; 159°08'E

522

524 **References**

- 525 Albani, S., Delmonte, B., Maggi, V., Baroni, C., Petit, J. R., Stenni, B., Mazzola, C., and Frezzotti, M.:
526 Interpreting last glacial to Holocene dust changes at Talos Dome (East Antarctica): implications for
527 atmospheric variations from regional to hemispheric scales, *Clim. Past*, 8, 741-750, 2012.
528
- 529 Amo, M. and Minagawa, M.: Sedimentary record of marine and terrigenous organic matter delivery to the
530 Shatsky Rise, western North Pacific, over the last 130 kyr, *Organic Geochemistry*, 34, 1299-1312, 2003.
531
- 532 Baccolo, G., Delmonte, B., Albani, S., Baroni, C., Cibin, G., Frezzotti, M., Hampai, D., Marcelli, A., Revel, M.,
533 and Salvatore, M.: Regionalization of the atmospheric dust cycle on the periphery of the East Antarctic ice
534 sheet since the last glacial maximum, *Geochemistry, Geophysics, Geosystems*, 19, 3540-3554, 2018.
535
- 536 Basile, I., Grousset, F. E., Revel, M., Petit, J. R., Biscaye, P. E., and Barkov, N. I.: Patagonian origin of glacial
537 dust deposited in East Antarctica (Vostok and Dome C) during glacial stages 2, 4 and 6, *Earth and Planetary
538 Science Letters*, 146, 573-589, 1997.
539
- 540 Boyd, P., Muggli, D., Varela, D., Goldblatt, R., Chretien, R., Orians, K., and Harrison, P.: In vitro iron
541 enrichment experiments in the NE subarctic Pacific, *Marine Ecology Progress Series*, 136, 179-193, 1996.
542
- 543 Burgay, F., Erhardt, T., Lunga, D. D., Jensen, C. M., Spolaor, A., Vallelonga, P., Fischer, H., and Barbante, C.:
544 Fe²⁺ in ice cores as a new potential proxy to detect past volcanic eruptions, *Science of The Total
545 Environment*, 654, 1110-1117, 2019.
546
- 547 Costa, K. M., McManus, J. F., and Anderson, R. F.: Paleoproductivity and Stratification Across the Subarctic
548 Pacific Over Glacial-Interglacial Cycles, *Paleoceanography and Paleoclimatology*, 33, 914-933, 2018.
549
- 550 Davies, M., Mix, A., Stoner, J., Addison, J., Jaeger, J., Finney, B., and Wiest, J.: The deglacial transition on the
551 southeastern Alaska Margin: Meltwater input, sea level rise, marine productivity, and sedimentary anoxia,
552 *Paleoceanography*, 26, 2011.
553
- 554 Delmonte, B., Andersson, P., Schöberg, H., Hansson, M., Petit, J., Delmas, R., Gaiero, D. M., Maggi, V., and
555 Frezzotti, M.: Geographic provenance of aeolian dust in East Antarctica during Pleistocene glaciations:
556 preliminary results from Talos Dome and comparison with East Antarctic and new Andean ice core data,
557 *Quaternary Science Reviews*, 29, 256-264, 2010a.
558
- 559 Delmonte, B., Baroni, C., Andersson, P. S., Schoberg, H., Hansson, M., Aciego, S., Petit, J.-R., Albani, S.,
560 Mazzola, C., Maggi, V., and Frezzotti, M.: Aeolian dust in the Talos Dome ice core (East Antarctica,
561 Pacific/Ross Sea sector): Victoria Land versus remote sources over the last two climate cycles, *Journal of
562 Quaternary Science*, 25, 1327-1337, 2010b.
563
- 564 Du, Z., Xiao, C., Mayewski, P. A., Handley, M. J., Li, C., Ding, M., Liu, J., Yang, J., and Liu, K.: The iron records
565 and its sources during 1990–2017 from the Lambert Glacial Basin shallow ice core, East Antarctica,
566 *Chemosphere*, 251, 126399, 2020.
567
- 568 Duggen, S., Olgun, N., Croot, P., Hoffmann, L. J., Dietze, H., Delmelle, P., and Teschner, C.: The role of
569 airborne volcanic ash for the surface ocean biogeochemical iron-cycle: a review, *Biogeosciences (BG)*, 7,
570 827-844, 2010.
571
- 572 Duprat, L. P., Bigg, G. R., and Wilton, D. J.: Enhanced Southern Ocean marine productivity due to
573 fertilization by giant icebergs, *Nature Geoscience*, 9, 219, 2016.
574

575 Edwards, R., Sedwick, P., Morgan, V., and Boutron, C.: Iron in ice cores from Law Dome: A record of
576 atmospheric iron deposition for maritime East Antarctica during the Holocene and Last Glacial Maximum,
577 *Geochemistry, Geophysics, Geosystems*, 7, 12, 2006.
578
579 Edwards, R., Sedwick, P. N., Morgan, V., Boutron, C. F., and Hong, S.: Iron in ice cores from Law Dome, East
580 Antarctica: implications for past deposition of aerosol iron, *Annals of Glaciology*, 27, 365-370, 1998.
581
582 Edwards, R. P. R.: Iron in modern and ancient East Antarctic snow: Implications for phytoplankton
583 production in the Southern Ocean, 1999. University of Tasmania, 1999.
584
585 Fuhrer, K., Wolff, E. W., and Johnsen, S. J.: Timescales for dust variability in the Greenland Ice Core Project
586 (GRIP) ice core in the last 100,000 years, *Journal of Geophysical Research: Atmospheres*, 104, 31043-31052,
587 1999.
588
589 Gaspari, V., Barbante, C., Cozzi, G., Cescon, P., Boutron, C., Gabrielli, P., Capodaglio, G., Ferrari, C., Petit, J.,
590 and Delmonte, B.: Atmospheric iron fluxes over the last deglaciation: Climatic implications, *Geophysical*
591 *Research Letters*, 33, 3, 2006.
592
593 Han, C., Do Hur, S., Han, Y., Lee, K., Hong, S., Erhardt, T., Fischer, H., Svensson, A. M., Steffensen, J. P., and
594 Vallelonga, P.: High-resolution isotopic evidence for a potential Saharan provenance of Greenland glacial
595 dust, *Scientific reports*, 8, 1-9, 2018.
596
597 Haug, G., Maslin, M., Sarnthein, M., Stax, R., and Tiedemann, R.: 20. EVOLUTION OF NORTHWEST PACIFIC
598 SEDIMENTATION PATTERNS SINCE 6 MA (SITE 882), 1995, 293.
599
600 Hiscock, W. T., Fischer, H., Bigler, M., Gfeller, G., Leuenberger, D., and Mini, O.: Continuous flow analysis of
601 labile iron in ice-cores, *Environmental science & technology*, 47, 4416-4425, 2013.
602
603 Jouzel, J., Waelbroeck, C., Malaize, B., Bender, M., Petit, J., Stievenard, M., Barkov, N., Barnola, J., King, T.,
604 and Kotlyakov, V.: Climatic interpretation of the recently extended Vostok ice records, *Climate Dynamics*,
605 12, 513-521, 1996.
606
607 Kang, S., Roberts, H. M., Wang, X., An, Z., and Wang, M.: Mass accumulation rate changes in Chinese loess
608 during MIS 2, and asynchrony with records from Greenland ice cores and North Pacific Ocean sediments
609 during the Last Glacial Maximum, *Aeolian Research*, 19, 251-258, 2015.
610
611 Kawahata, H., Okamoto, T., Matsumoto, E., and Ujiie, H.: Fluctuations of eolian flux and ocean productivity
612 in the mid-latitude North Pacific during the last 200 kyr, *Quaternary Science Reviews*, 19, 1279-1291, 2000.
613
614 Kienast, S. S., Hendy, I. L., Crusius, J., Pedersen, T. F., and Calvert, S. E.: Export production in the subarctic
615 North Pacific over the last 800 kyrs: No evidence for iron fertilization?, *Journal of Oceanography*, 60, 189-
616 203, 2004.
617
618 Koffman, B. G., Handley, M. J., Osterberg, E. C., Wells, M. L., and Kreutz, K. J.: Dependence of ice-core
619 relative trace-element concentration on acidification, *Journal of Glaciology*, 60, 103-112, 2014.
620
621 Kohfeld, K. E. and Chase, Z.: Temporal evolution of mechanisms controlling ocean carbon uptake during the
622 last glacial cycle, *Earth and Planetary Science Letters*, 472, 206-215, 2017.
623
624 Köhler, P., Nehrbass-Ahles, C., Schmitt, J., Stocker, T. F., and Fischer, H.: Continuous record of the
625 atmospheric greenhouse gas carbon dioxide (CO₂), raw data. In: In supplement to: Köhler, P et al. (2017): A
626 156 kyr smoothed history of the atmospheric greenhouse gases CO₂, CH₄, and N₂O and their radiative

627 forcing. *Earth System Science Data*, 9(1), 363-387, <https://doi.org/10.5194/essd-9-363-2017>, PANGAEA,
628 2017.
629

630 Lam, P. and Bishop, J. K. B.: The continental margin is a key source of iron to the HNLC North Pacific Ocean,
631 *Geophysical Research Letters*, 35, 7, 2008.
632

633 Lambert, F., Delmonte, B., Petit, J.-R., Bigler, M., Kaufmann, P. R., Hutterli, M. A., Stocker, T. F., Ruth, U.,
634 Steffensen, J. P., and Maggi, V.: Dust-climate couplings over the past 800,000 years from the EPICA Dome C
635 ice core, *Nature*, 452, 616, 2008.
636

637 Lambert, F., Tagliabue, A., Shaffer, G., Lamy, F., Winckler, G., Farias, L., Gallardo, L., and De Pol-Holz, R.:
638 Dust fluxes and iron fertilization in Holocene and Last Glacial Maximum climates, *Geophysical Research*
639 *Letters*, 42, 6014-6023, 2015.
640

641 Langmann, B., Zakšek, K., Hort, M., and Duggen, S.: Volcanic ash as fertiliser for the surface ocean,
642 *Atmospheric Chemistry and Physics*, 10, 3891-3899, 2010.
643

644 Löfverström, M., Caballero, R., Nilsson, J., and Kleman, J.: Evolution of the large-scale atmospheric
645 circulation in response to changing ice sheets over the last glacial cycle, *Climate of the Past*, 10, 1453-1471,
646 2014.
647

648 Lupker, M., Aciego, S. M., Bourdon, B., Schwander, J., and Stocker, T.: Isotopic tracing (Sr, Nd, U and Hf) of
649 continental and marine aerosols in an 18th century section of the Dye-3 ice core (Greenland), *Earth and*
650 *Planetary Science Letters*, 295, 277-286, 2010.
651

652 Mahowald, N. M., Engelstaedter, S., Luo, C., Sealy, A., Artaxo, P., Benitez-Nelson, C., Bonnet, S., Chen, Y.,
653 Chuang, P. Y., Cohen, D. D., Dulac, F., Herut, B., Johansen, A. M., Kubilay, N., Losno, R., Maenhaut, W.,
654 Paytan, A., Prospero, J. M., Shank, L. M., and Siefert, R. L.: Atmospheric Iron Deposition: Global Distribution,
655 Variability, and Human Perturbations, *Annual Review of Marine Science*, 1, 245-278, 2008.
656

657 Mahowald, N. M., Yoshioka, M., Collins, W. D., Conley, A. J., Fillmore, D. W., and Coleman, D. B.: Climate
658 response and radiative forcing from mineral aerosols during the last glacial maximum, pre-industrial,
659 current and doubled-carbon dioxide climates, *Geophysical Research Letters*, 33, 2006.
660

661 Manabe, S. and Broccoli, A.: The influence of continental ice sheets on the climate of an ice age, *Journal of*
662 *Geophysical Research: Atmospheres*, 90, 2167-2190, 1985.
663

664 Martin, J. H., Gordon, R. M., and Fitzwater, S. E.: Iron in Antarctic waters, *Nature*, 345, 156-158, 1990.
665 Martínez-García, A., Rosell-Melé, A., Jaccard, S. L., Geibert, W., Sigman, D. M., and Haug, G. H.: Southern
666 Ocean dust-climate coupling over the past four million years, *Nature*, 476, 312, 2011.
667

668 Martínez-García, A., Sigman, D. M., Ren, H., Anderson, R. F., Straub, M., Hodell, D. A., Jaccard, S. L.,
669 Eglinton, T. I., and Haug, G. H.: Iron fertilization of the Subantarctic Ocean during the last ice age, *Science*,
670 343, 1347-1350, 2014.
671

672 Mayewski, P. A., Meeker, L. D., Whitlow, S., Twickler, M. S., Morrison, M. C., Bloomfield, P., Bond, G., Alley,
673 R. B., Gow, A. J., and Meese, D. A.: Changes in atmospheric circulation and ocean ice cover over the North
674 Atlantic during the last 41,000 years, *Science*, 263, 1747-1751, 1994.
675

676 McDonald, D., Pedersen, T., and Crusius, J.: Multiple late Quaternary episodes of exceptional diatom
677 production in the Gulf of Alaska, *Deep Sea Research Part II: Topical Studies in Oceanography*, 46, 2993-
678 3017, 1999.
679

680 McManus, J. F., Francois, R., Gherardi, J.-M., Keigwin, L. D., and Brown-Leger, S.: Collapse and rapid
681 resumption of Atlantic meridional circulation linked to deglacial climate changes, *Nature*, 428, 834-837,
682 2004.
683
684 Méheust, M., Stein, R., Fahl, K., and Gersonde, R.: Sea-ice variability in the subarctic North Pacific and
685 adjacent Bering Sea during the past 25 ka: new insights from IP 25 and U k' 37 proxy records, *arktos*, 4, 8,
686 2018.
687
688 Méheust, M., Stein, R., Fahl, K., Max, L., and Riethdorf, J.-R.: High-resolution IP 25-based reconstruction of
689 sea-ice variability in the western North Pacific and Bering Sea during the past 18,000 years, *Geo-Marine*
690 *Letters*, 36, 101-111, 2016.
691
692 Miller, R. and Tegen, I.: Climate response to soil dust aerosols, *Journal of climate*, 11, 3247-3267, 1998.
693 Müller, J., Wagner, A., Fahl, K., Stein, R., Prange, M., and Lohmann, G.: Towards quantitative sea ice
694 reconstructions in the northern North Atlantic: A combined biomarker and numerical modelling approach,
695 *Earth and Planetary Science Letters*, 306, 137-148, 2011.
696
697 North Greenland Ice Core Project, M.: 50 year means of oxygen isotope data from ice core NGRIP. In:
698 Supplement to: North Greenland Ice Core Project Members (2004): High-resolution record of Northern
699 Hemisphere climate extending into the last interglacial period. *Nature*, 431, 147-151,
700 <https://doi.org/10.1038/nature02805>, PANGAEA, 2007.
701
702 Olgun, N., Duggen, S., Croot, P. L., Delmelle, P., Dietze, H., Schacht, U., Oskarsson, N., Siebe, C., Auer, A.,
703 and Garbe-Schönberg, D.: Surface ocean iron fertilization: the role of subduction zone and hotspot volcanic
704 ash and fluxes into the Pacific Ocean, *Global Biogeochemical Cycles*, 25, GB4001, 2011.
705
706 Rasmussen, S. O., Abbott, P. M., Blunier, T., Bourne, A. J., Brook, E., Buchardt, S. L., Buizert, C., Chappellaz,
707 J., Clausen, H. B., Cook, E., Dahl-Jensen, D., Davies, S. M., Guillevic, M., Kipfstuhl, S., Laepple, T., Seierstad, I.
708 K., Severinghaus, J. P., Steffensen, J. P., Stowasser, C., Svensson, A., Vallelonga, P., Vinther, B. M., Wilhelms,
709 F., and Winstrup, M.: A first chronology for the North Greenland Eemian Ice Drilling (NEEM) ice core, *Clim.*
710 *Past*, 9, 2713-2730, 2013.
711
712 Ren, H., Studer, A. S., Serno, S., Sigman, D. M., Winckler, G., Anderson, R. F., Oleynik, S., Gersonde, R., and
713 Haug, G. H.: Glacial-to-interglacial changes in nitrate supply and consumption in the subarctic North Pacific
714 from microfossil-bound N isotopes at two trophic levels, *Paleoceanography*, 30, 1217-1232, 2015.
715 Röthlisberger, R.: Ice core evidence for the extent of past atmospheric CO₂ change due to iron fertilisation,
716 *Geophysical Research Letters*, 31, 16, 2004.
717
718 Ruth, U.: Dust concentration in the NGRIP ice core. In: Supplement to: Ruth, Urs; Bigler, Matthias;
719 Röthlisberger, Regine; Siggaard-Andersen, Marie-Louise; Kipfstuhl, Sepp; Goto-Azuma, Kumiko; Hansson,
720 Margareta E; Johnsen, Sigfus J; Lu, Huayu; Steffensen, Jørgen Peder (2007): Ice core evidence for a very
721 tight link between North Atlantic and east Asian glacial climate. *Geophysical Research Letters*, 34, L03706,
722 <https://doi.org/10.1029/2006GL027876>, PANGAEA, 2007.
723
724 Ruth, U., Bigler, M., Röthlisberger, R., Siggaard-Andersen, M. L., Kipfstuhl, S., Goto-Azuma, K., Hansson, M.
725 E., Johnsen, S. J., Lu, H., and Steffensen, J. P.: Ice core evidence for a very tight link between North Atlantic
726 and east Asian glacial climate, *Geophysical Research Letters*, 34, 2007.
727
728 Sachs, J. P. and Anderson, R. F.: Increased productivity in the subantarctic ocean during Heinrich events,
729 *Nature*, 434, 1118-1121, 2005.
730
731 Schepanski, K.: Transport of mineral dust and its impact on climate, *Geosciences*, 8, 151, 2018.
732

733 Schüpbach, S., Fischer, H., Bigler, M., Erhardt, T., Gfeller, G., Leuenberger, D., Mini, O., Mulvaney, R.,
734 Abram, N. J., and Fleet, L.: Greenland records of aerosol source and atmospheric lifetime changes from the
735 Eemian to the Holocene, *Nature communications*, 9, 1476, 2018.

736

737 Serno, S., Winckler, G., Anderson, R. F., Hayes, C. T., McGee, D., Machalett, B., Ren, H., Straub, S. M.,
738 Gersonde, R., and Haug, G. H.: Eolian dust input to the Subarctic North Pacific, *Earth and Planetary Science
739 Letters*, 387, 252-263, 2014.

740

741 Serno, S., Winckler, G., Anderson, R. F., Maier, E., Ren, H., Gersonde, R., and Haug, G. H.: Comparing dust
742 flux records from the Subarctic North Pacific and Greenland: Implications for atmospheric transport to
743 Greenland and for the application of dust as a chronostratigraphic tool, *Paleoceanography*, 30, 583-600,
744 2015.

745

746 Shoenfelt, E. M., Sun, J., Winckler, G., Kaplan, M. R., Borunda, A. L., Farrell, K. R., Moreno, P. I., Gaiero, D.
747 M., Recasens, C., and Sambrotto, R. N.: High particulate iron (II) content in glacially sourced dusts enhances
748 productivity of a model diatom, *Science advances*, 3, e1700314, 2017.

749

750 Shoenfelt, E. M., Winckler, G., Lamy, F., Anderson, R. F., and Bostick, B. C.: Highly bioavailable dust-borne
751 iron delivered to the Southern Ocean during glacial periods, *Proceedings of the National Academy of
752 Sciences*, 115, 11180-11185, 2018.

753

754 Smetacek, V., Klaas, C., Strass, V. H., Assmy, P., Montresor, M., Cisewski, B., Savoye, N., Webb, A., d'Ovidio,
755 F., and Arrieta, J. M.: Deep carbon export from a Southern Ocean iron-fertilized diatom bloom, *Nature*, 487,
756 313-319, 2012.

757

758 Spolaor, A., Vallelonga, P., Cozzi, G., Gabrieli, J., Varin, C., Kehrwald, N., Zennaro, P., Boutron, C., and
759 Barbante, C.: Iron speciation in aerosol dust influences iron bioavailability over glacial-interglacial
760 timescales, *Geophysical Research Letters*, 40, 1618-1623, 2013.

761

762 Sun, W., Shen, J., Yu, S.-Y., Long, H., Zhang, E., Liu, E., and Chen, R.: A lacustrine record of East Asian
763 summer monsoon and atmospheric dust loading since the last interglaciation from Lake Xingkai, northeast
764 China, *Quaternary Research*, 89, 270-280, 2018.

765

766 Svensson, A., Biscaye, P. E., and Grousset, F. E.: Characterization of late glacial continental dust in the
767 Greenland Ice Core Project ice core, *Journal of Geophysical Research: Atmospheres*, 105, 4637-4656, 2000.

768 Talley, L. D.: Freshwater transport estimates and the global overturning circulation: Shallow, deep and
769 throughflow components, *Progress in Oceanography*, 78, 257-303, 2008.

770

771 Tsuda, A., Takeda, S., Saito, H., Nishioka, J., Nojiri, Y., Kudo, I., Kiyosawa, H., Shiimoto, A., Imai, K., and Ono,
772 T.: A mesoscale iron enrichment in the western subarctic Pacific induces a large centric diatom bloom,
773 *Science*, 300, 958-961, 2003.

774

775 Tulenko, J. P., Lofverstrom, M., and Briner, J. P.: Ice sheet influence on atmospheric circulation explains the
776 patterns of Pleistocene alpine glacier records in North America, *Earth and Planetary Science Letters*, 534,
777 116115, 2020.

778

779 Vallelonga, P., Barbante, C., Cozzi, G., Gabrieli, J., Schüpbach, S., Spolaor, A., and Turetta, C.: Iron fluxes to
780 Talos Dome, Antarctica, over the past 200 kyr, *Clim. Past*, 9, 597-604, 2013.

781

782 Vallelonga, P., Van de Velde, K., Candelone, J.-P., Morgan, V., Boutron, C., and Rosman, K.: The lead
783 pollution history of Law Dome, Antarctica, from isotopic measurements on ice cores: 1500 AD to 1989 AD,
784 *Earth and Planetary Science Letters*, 204, 291-306, 2002.

785

786 Watanabe, O., Jouzel, J., Johnsen, S., Parrenin, F., Shoji, H., and Yoshida, N.: Homogeneous climate
787 variability across East Antarctica over the past three glacial cycles, *Nature*, 422, 509-512, 2003.
788

789 Wolff, E. W., Fischer, H., Fundel, F., Ruth, U., Twarloh, B., Littot, G. C., Mulvaney, R., Röthlisberger, R., De
790 Angelis, M., and Boutron, C. F.: Southern Ocean sea-ice extent, productivity and iron flux over the past
791 eight glacial cycles, *Nature*, 440, 491-496, 2006.
792

793 Xiao, C., Du, Z., Handley, M. J., Mayewski, P. A., Cao, J., Schüpbach, S., Zhang, T., Petit, J.-R., Li, C., and Han,
794 Y.: Iron in the NEEM ice core relative to Asian loess records over the last glacial-interglacial cycle, *National
795 Science Review*, 2020. 2020.
796

797 Xiao, J., An, Z., Liu, T., Inouchi, Y., Kumai, H., Yoshikawa, S., and Kondo, Y.: East Asian monsoon variation
798 during the last 130,000 years: evidence from the Loess Plateau of central China and Lake Biwa of Japan,
799 *Quaternary Science Reviews*, 18, 147-157, 1999.
800

801 Yoon, J.-E., Yoo, K.-C., Macdonald, A. M., Yoon, H.-I., Park, K.-T., Yang, E. J., Kim, H.-C., Lee, J. I., Lee, M. K.,
802 and Jung, J.: Reviews and syntheses: Ocean iron fertilization experiments—past, present, and future looking
803 to a future Korean Iron Fertilization Experiment in the Southern Ocean (KIFES) project, *Biogeosciences*, 15,
804 5847-5889, 2018.
805

806 Young, R., Carder, K., Betzer, P., Costello, D., Duce, R., DiTullio, G., Tindale, N., Laws, E., Uematsu, M., and
807 Merrill, J.: Atmospheric iron inputs and primary productivity: Phytoplankton responses in the North Pacific,
808 *Global Biogeochemical Cycles*, 5, 119-134, 1991.
809

810 Yung, Y. L., Lee, T., Wang, C.-H., and Shieh, Y.-T.: Dust: A diagnostic of the hydrologic cycle during the Last
811 Glacial Maximum, *Science*, 271, 962-963, 1996.
812

813 Zahn, R., Pedersen, T. F., Bornhold, B. D., and Mix, A. C.: Water mass conversion in the glacial subarctic
814 Pacific (54° N, 148° W): Physical constraints and the benthic-planktonic stable isotope record,
815 *Paleoceanography*, 6, 543-560, 1991.
816

817 Zhang, X.-Y., Gong, S., Zhao, T., Arimoto, R., Wang, Y., and Zhou, Z.: Sources of Asian dust and role of
818 climate change versus desertification in Asian dust emission, *Geophysical Research Letters*, 30, 2003.
819

820 Zhang, X., Han, Y., Sun, Y., Cao, J., and An, Z.: Asian dust, eolian iron and black carbon—Connections to
821 climate changes. In: *Late Cenozoic Climate Change in Asia*, Springer, 2014.
822

823